RESEARCH   **Open Access**

Instantaneous cross-correlation function type of WD based LFM signals analysis via output SNR inequality modeling

Sheng-Zhou Qiang[1], Xian Jiang[1], Pu-Yu Han[1], Xi-Ya Shi[1], An-Yang Wu[1], Yun Sun[1], Yun-Jie Chen[1] and Zhi-Chao Zhang[1,2]*

*Correspondence:
zzc910731@163.com
[1] School of Mathematics and Statistics, Nanjing University of Information Science and Technology, Nanjing 210044, China Full list of author information is available at the end of the article

Abstract

Linear canonical transform (LCT) is a powerful tool for improving the detection accuracy of the conventional Wigner distribution (WD). However, the LCT free parameters embedded increase computational complexity. Recently, the instantaneous cross-correlation function type of WD (ICFWD), a specific WD relevant to the LCT, has shown to be an outcome of the tradeoff between detection accuracy and computational complexity. In this paper, the ICFWD is applied to detect noisy single component and bi-component linear frequency-modulated (LFM) signals through the output signal-to-noise ratio (SNR) inequality modeling and solving with respect to the ICFWD and WD. The expectation-based output SNR inequality model between the ICFWD and WD on a pure deterministic signal added with a zero-mean random noise is proposed. The solutions of the inequality model in regard to single component and bi-component LFM signals corrupted with additive zero-mean stationary noise are obtained respectively. The detection accuracy of ICFWD with that of the closed-form ICFWD (CICFWD), the affine characteristic Wigner distribution (ACWD), the kernel function Wigner distribution (KFWD), the convolution representation Wigner distribution (CRWD) and the classical WD is compared. It also compares the computing speed of ICFWD with that of CICFWD, ACWD, KFWD and CRWD.

Keywords: Computational complexity, Detection accuracy, Instantaneous cross-correlation function, Linear canonical Wigner distribution, Weak signal detection

1 Introduction

In recent decades, the linear canonical transform (LCT) has been attracted much attention due to its significance in optics propagation [1], time-frequency analysis [2], and signal processing [3]. Some well-known integral transformations, including Fourier transform (FT) [4], fractional Fourier transform (FRFT) [5–9], Fresnel transform [10] and Lorentz transform [11], are special cases of the LCT. The generalizability of LCT enables it to be a representative integral transformation. The LCT has three free parameters, which outperforms the FT without any degrees of freedom and the FRFT with only one degree of freedom in non-stationary signal analysis. Indeed, the LCT

Qiang *et al. EURASIP Journal on Advances in Signal Processing* (2021) 2021:122

Page 2 of 24

exhibits more flexibility in signal representation through a so-called linear canonical domain beyond the ordinary time, frequency and fractional domains.

Wigner distribution (WD) began its definition at quantum statistical mechanics [12] and later had found many applications in signal processing [13]. As it is known, the WD is an effective time-frequency analysis tool but subjected to the interference of the cross-term when dealing with multi-component signals. This kind of issue is the subject which the WD pays attention throughout. As a result, a large number of variations to the WD are currently derived, including pseudo Wigner distribution [14], smoothed pseudo Wigner distribution [15], S-method [16], general Wigner distribution [17], *L* Wigner distribution [18], Choi-Williams distribution [19], and scaled Wigner distribution [20]. These variations are both energy distributions in the time-frequency plane. Take the sky-wave over-the-horizon radar signal detection [21] for example, however, without any degrees of freedom they fail to extract principal features of the target echo signal from the extreme strong noise background. To address the problem of weak signal detection [22], ones need some breakthrough research approaches to extend the conventional WD.

From the perspective of improving signal representation flexibility, it seems a feasible method for the detection problem of weak signals to introduce the parameters of LCT into the conventional WD. There exist various types of parameters embedded technologies, such as linear canonical domain autocorrelation function replacement [2], linear canonical domain kernel replacement [23–25], linear canonical domain convolution replacement [26], linear canonical domain instantaneous cross-correlation function (ICF) replacement [27], and linear canonical domain closed-form instantaneous cross-correlation function (CICF) replacement [28]. The corresponding variations of the WD are referred to as the affine characteristic Wigner distribution (ACWD) [2], the kernel function Wigner distribution (KFWD) [23], the convolution representation Wigner distribution (CRWD) [26], the ICF type of Wigner distribution (ICFWD) [27], and the CICF type of Wigner distribution (CICFWD) [28], respectively.

The numbers of LCT free parameters of the ACWD, KFWD, CRWD, ICFWD and CICFWD are three, three, three, six and nine, respectively. The more the number of parameters the time-frequency distribution has, the more flexible the signal representation is. In this case, the detection accuracy will be better. Therefore, our previous works focused mainly on the CICFWD-based weak signal detection. To be specific, we established an output signal-to-noise ratio (SNR) inequality [29] (inequalities system [30]) model or optimization [31] (multiobjective optimization [32]) model of the CICFWD to explain why its detection accuracy improves. Also, we solved the inequality (inequalities system) model or optimization (multiobjective optimization) model for noisy linear frequency-modulated (LFM) signals [33–35] to verify the improvement of detection accuracy. However, there exist two problems caused by too many parameters. The parameters selection strategy of CICFWD is not unique so that there is an unstable detection accuracy [36]. The CICFWD's high complexity and low computation efficiency make it not suitable for real-time applications [37]. For the options with less parameters, there are the ACWD, KFWD, CRWD, and ICFWD. It is therefore wise to choose the ICFWD for maintaining a high level of detection accuracy as possible, because the number of its parameters is the largest among them.

Qiang *et al. EURASIP Journal on Advances in Signal Processing*   (2021) 2021:122

Page 3 of 24

In our latest works, the output SNR optimization [37] and multiobjective optimization [36] models of the ICFWD were formulated respectively. The optimal solutions of the models with respect to noisy single component LFM signal were also derived. It was crucially used there that only one absolute value term can be found in the objective function for the single component LFM signal. Then Lagrangian multiplier method [38] works very well by merely squaring the objective function. This method thereby relies heavily on the fact that the LFM signal is single component which does not seem to work for multi-component LFM signals, for which there is more than one absolute value term found in the objective function. To overcome this shortcoming, it might be feasible to replace the optimization model with the inequality model as solving the inequality model does not need to use Lagrangian multiplier method.

The main purpose of this paper is to study weak signal detection problem through the output SNR inequality modeling and solving of the ICFWD. We first propose an output SNR inequality model of the ICFWD. We then solve the inequality model in regard to both single component and bi-component LFM signals under a zero-mean stationary noise background. We also compare the detection accuracy of ICFWD, CICFWD, ACWD, KFWD, CRWD and WD, as well as the computing speed of ICFWD, CICFWD, ACWD, KFWD and CRWD. The main notations are summarized in Table 1.

The main contributions of this paper are summarized below:

Table 1 Summary of main notations

Notation	Description
$f, f_1, \widehat{g}, \widetilde{g}; n$	Deterministic signals; random noise
$\mathbf{A} = (a, b; c, d), \mathbf{A}_1 = (a_1, b_1; c_1, d_1), \mathbf{A}_2 = (a_2, b_2; c_2, d_2)$	Parameter matrices
$\mathcal{K}_{\mathbf{A}}, \mathcal{K}_{\mathbf{A}_1}$	Linear canonical domain kernel functions
$F_{\mathbf{A}}, F_{\mathbf{A}_1}, F_{\mathbf{A}_2}; \widehat{G}_{\mathbf{A}_1}; \widetilde{G}_{\mathbf{A}_1}$	LCTs of f; LCT of $\widehat{g}$; LCT of $\widetilde{g}$
$*$	Complex conjugate
$f\left(t + \frac{\tau}{2}\right)f^*\left(t - \frac{\tau}{2}\right)$	Instantaneous autocorrelation function
$F_{\mathbf{A}_1}\left(t + \frac{\tau}{2}\right)f^*\left(t - \frac{\tau}{2}\right), \widehat{G}_{\mathbf{A}_1}\left(t + \frac{\pi}{2}\right)\widehat{g}^*\left(t - \frac{\pi}{2}\right), \widetilde{G}_{\mathbf{A}_1}\left(t + \frac{\pi}{2}\right)\widehat{g}^*\left(t - \frac{\pi}{2}\right)$	Linear canonical domain ICFs
$F_{\mathbf{A}_1}\left(t + \frac{\tau}{2}\right)F_{\mathbf{A}_2}^*\left(t - \frac{\tau}{2}\right)$	Linear canonical domain CICF
W_f, W_n	WDs of f, n
$W_f^{\mathbf{A}_1, \mathbf{A}_2, \mathbf{A}}, W_n^{\mathbf{A}_1, \mathbf{A}_2, \mathbf{A}}, W_{f+n}^{\mathbf{A}_1, \mathbf{A}_2, \mathbf{A}}$	CICFWDs of $f, n, f + n$
$W_f^{\mathbf{A}_1, \mathbf{A}}, W_{\widehat{g}}^{\mathbf{A}_1, \mathbf{A}}, W_{\widetilde{g}}^{\mathbf{A}_1, \mathbf{A}}, W_n^{\mathbf{A}_1, \mathbf{A}}, W_{f+n}^{\mathbf{A}_1, \mathbf{A}}$	ICFWDs of $f, \widehat{g}, \widetilde{g}, n, f + n$
$W_{\widehat{g}\widetilde{g}}^{\mathbf{A}_1, \mathbf{A}}, W_{\widetilde{g}\widehat{g}}^{\mathbf{A}_1, \mathbf{A}}$	Cross ICFWDs of $\widehat{g}$ and $\widetilde{g}$
$\text{ESNR}_{\text{WD}}, \text{ESNR}_{\text{ICFWD}}^{\mathbf{A}_1, \mathbf{A}}, \text{ESNR}_{\text{CICFWD}}^{\mathbf{A}_1, \mathbf{A}_2, \mathbf{A}}$	Expectation-based output SNRs of WD, ICFWD, CICFWD
max; arg max	Maximum; arguments of the maximum
Mean	Arithmetic mean or integral average
$\text{E}[\cdot]; \text{Var}[\cdot]$	Expectation operator; variance operator
$\delta(\cdot)$	Dirac delta operator
$\alpha, \widehat{\alpha}, \widetilde{\alpha}; \beta, \widehat{\beta}, \widetilde{\beta}$	Initial frequency; frequency rate
$h_1, \widehat{h}_1, \widetilde{h}_1$	$\frac{1}{2\beta b_1 + a_1}, \frac{1}{2\widehat{\beta} b_1 + a_1}, \frac{1}{2\widetilde{\beta} b_1 + a_1}$
$\widetilde{\widetilde{l}}, \widehat{\widehat{l}}$	$\frac{a}{2b} + \frac{d_1 - \widehat{h}_1}{8b_1} - \frac{\widetilde{\beta}}{4}, \frac{a}{2b} + \frac{d_1 - \widehat{h}_1}{8b_1} - \frac{\widehat{\beta}}{4}$
D	Power spectral density of the noise

- It formulates the expectation-based output SNR of ICFWD for pure deterministic signal embedded in additive zero-mean random noise.
- It establishes the expectation-based output SNR inequality model between the ICFWD and WD on the noisy signal.
- It deduces the solutions of the inequality model for single component and bi-component LFM signals added with zero-mean stationary noise, respectively.
- It demonstrates the advantages of ICFWD in maintaining/improving detection accuracy and saving computing time.

The remainder of this paper is structured as follows. Section 2 reviews the definitions of LCT and ICFWD. Section 3 investigates the expectation-based output SNR inequality modeling and solving of the ICFWD. Section 4 derives the solutions of the inequality model for noisy LFM signals. Section 5 conducts numerical experiments. Section 6 concludes the paper.

2 Preliminaries

2.1 Linear canonical transform (LCT)

From the view point of geometry, the FT and FRFT are rotation transformations with the angles of $\frac{\pi}{2}$ and α in the time-frequency plane, respectively. The LCT, a generalization of the FRFT or known as extended FRFT, can be regarded as an affine transformation in the time-frequency plane [39–42]. The LCT of a signal $f(t)$ relevant to the parameter matrix $\mathbf{A} = (a, b; c, d)$ is defined by [43–48]

$$
F_{\mathbf{A}}(u) = \begin{cases} \int_{-\infty}^{+\infty} f(t)\mathcal{K}_{\mathbf{A}}(u,t)\mathrm{d}t, & b \neq 0 \\ \sqrt{d}\mathrm{e}^{\mathrm{j}\frac{cd}{2}u^2}f(du), & b = 0 \end{cases}, \tag{1}
$$

where

$$
\mathcal{K}_{\mathbf{A}}(u,t) = \frac{1}{\sqrt{\mathrm{j}2\pi b}}\mathrm{e}^{\mathrm{j}\left(\frac{d}{2b}u^2 - \frac{1}{b}ut + \frac{a}{2b}t^2\right)} \tag{2}
$$

denotes the linear canonical domain kernel function. The parameters a, b, c, d are real numbers satisfying the affine condition $ad - bc = 1$.

Two special cases of LCT are worth emphasizing as follows. Firstly, the LCT with $\mathbf{A} = (1, 0; 0, 1)$ reduces to a unit transformation, that is $F_{(1,0;0,1)}(u) = f(u)$. Secondly, the LCT with $\mathbf{A} = (0, 1; -1, 0)$ turns into the conventional FT, regardless of an extra constant factor $\frac{1}{\sqrt{\mathrm{j}}}$, that is $F_{(0,1;-1,0)}(u) = \frac{1}{\sqrt{\mathrm{j}2\pi}}\int_{-\infty}^{+\infty} f(t)\mathrm{e}^{-\mathrm{j}ut}\mathrm{d}t$.

The LCT with $b = 0$ is just a combination of a scaling operation $\sqrt{d}f(du)$ and a chirp multiplication operation $\mathrm{e}^{\mathrm{j}\frac{cd}{2}u^2}$. The LCT with $a = 0$ is none other than a combination of a scaling FT operation $\frac{1}{\sqrt{b}}F_{(0,1;-1,0)}\left(\frac{u}{b}\right)$ and a chirp multiplication operation $\mathrm{e}^{\mathrm{j}\frac{d}{2b}u^2}$. Then, the linear canonical domains with $b = 0$ and $a = 0$ become the ordinary time and frequency domains, respectively. Without loss of generality, this paper therefore discusses merely on the LCT with $b \neq 0$ and $a \neq 0$. The three free parameters of LCT are a, b, d or a, b, c, because it derives from $ad - bc = 1$ and $b \neq 0$ or $a \neq 0$ that $c = \frac{ad-1}{b}$ or $d = \frac{bc+1}{a}$.

2.2 ICF type of WD (ICFWD)

Let $F_{\mathbf{A}_1}\left(t+\frac{\tau}{2}\right)f^*\left(t-\frac{\tau}{2}\right)$ denote the linear canonical domain ICF, where $F_{\mathbf{A}_1}$ stands for the LCT of $f(t)$ relevant to the parameter matrix $\mathbf{A}_1 = (a_1, b_1; c_1, d_1)$, and the superscript $*$ is complex conjugate. Then, the ICFWD of $f(t)$ is defined by the LCT of $F_{\mathbf{A}_1}\left(t+\frac{\tau}{2}\right)f^*\left(t-\frac{\tau}{2}\right)$ relevant to the parameter matrix $\mathbf{A}$, i.e. [27],

$$W_f^{\mathbf{A}_1,\mathbf{A}}(t,u) = \int_{-\infty}^{+\infty} F_{\mathbf{A}_1}\left(t+\frac{\tau}{2}\right)f^*\left(t-\frac{\tau}{2}\right)\mathcal{K}_{\mathbf{A}}(u,\tau)\mathrm{d}\tau. \tag{3}$$

Two parameter matrices $\mathbf{A}_1, \mathbf{A}$ implies that the ICFWD has six LCT free parameters.

Let $F_{\mathbf{A}_2}$ denote the LCT of $f(t)$ relevant to the parameter matrix $\mathbf{A}_2 = (a_2, b_2; c_2, d_2)$. By replacing the linear canonical domain ICF $F_{\mathbf{A}_1}\left(t+\frac{\tau}{2}\right)f^*\left(t-\frac{\tau}{2}\right)$ with the linear canonical domain CICF $F_{\mathbf{A}_1}\left(t+\frac{\tau}{2}\right)F_{\mathbf{A}_2}^*\left(t-\frac{\tau}{2}\right)$, it follows the definition of the CICFWD of $f(t)$ [28–32]

$$W_f^{\mathbf{A}_1,\mathbf{A}_2,\mathbf{A}}(t,u) = \int_{-\infty}^{+\infty} F_{\mathbf{A}_1}\left(t+\frac{\tau}{2}\right)F_{\mathbf{A}_2}^*\left(t-\frac{\tau}{2}\right)\mathcal{K}_{\mathbf{A}}(u,\tau)\mathrm{d}\tau. \tag{4}$$

It is none other than the LCT of $F_{\mathbf{A}_1}\left(t+\frac{\tau}{2}\right)F_{\mathbf{A}_2}^*\left(t-\frac{\tau}{2}\right)$ relevant to the parameter matrix $\mathbf{A}$. There are three parameter matrices $\mathbf{A}_1, \mathbf{A}_2, \mathbf{A}$ so that the CICFWD has nine LCT free parameters.

The ICFWD exhibits less computational complexity than the CICFWD due to no calculations for $F_{\mathbf{A}_2}$. This is the main reason why the paper use the ICFWD to improve the efficiency of weak signal detection. Moreover, the ICFWD is not a special case of the CICFWD because of an assumption of $b_2 \neq 0$. Then, the ICFWD maybe could share the same level of detection accuracy in comparison with the CICFWD.

The ICFWD with $\mathbf{A}_1 = (1, 0; 0, 1)$ and $\mathbf{A} = (0, 1; -1, 0)$ becomes the conventional WD [13]

$$W_f(t,\omega) = \int_{-\infty}^{+\infty} f\left(t+\frac{\tau}{2}\right)f^*\left(t-\frac{\tau}{2}\right)\mathrm{e}^{-j\omega\tau}\mathrm{d}\tau, \tag{5}$$

regardless of an extra constant factor $\frac{1}{\sqrt{j2\pi}}$. Compared with the WD, the ICFWD achieves more degrees of freedom to improve the accuracy of weak signal detection.

3 Mathematical model

In this section, we first define the expectation-based output SNR of ICFWD for a general noisy signal modeled by a pure deterministic signal $f(t)$ added with a zero-mean random noise $n(t)$. We then establish the expectation-based output SNR inequality model between the ICFWD and WD. Finally, we study how to solve the inequality model from the perspective of signal forms including synthetic signals and real-world signals.

3.1 Expectation-based output SNR of ICFWD

Let the noisy signal be $f(t) + n(t)$, where $f(t)$ and $n(t)$ denote a pure deterministic signal and a zero-mean random noise, respectively. Then, the expectation-based output SNR of CICFWD is reproduced here as [29], Eq. (32)]

$$\text{ESNR}_{\text{CICFWD}}^{\mathbf{A}_1,\mathbf{A}_2,\mathbf{A}} = \frac{\max\limits_{(t,u)\in\mathbb{R}^2} \left| W_f^{\mathbf{A}_1,\mathbf{A}_2,\mathbf{A}}(t,u) \right|}{\underset{\underset{(t,u)}{\arg\max} \left| W_f^{\mathbf{A}_1,\mathbf{A}_2,\mathbf{A}}(t,u) \right|}{\text{Mean}} \left\{ \left| E\left[W_n^{\mathbf{A}_1,\mathbf{A}_2,\mathbf{A}}(t,u) \right] \right| \right\}}, \tag{6}$$

where 'Mean' would be the arithmetic mean if $\arg\max\limits_{(t,u)} \left| W_f^{\mathbf{A}_1,\mathbf{A}_2,\mathbf{A}}(t,u) \right|$ were a countable set, while the integral average if it were an uncountable set.

Note that the expectation-based output SNR of CICFWD is well-defined thanks to an important relation $E\left[W_{f+n}^{\mathbf{A}_1,\mathbf{A}_2,\mathbf{A}}(t,u) \right] = W_f^{\mathbf{A}_1,\mathbf{A}_2,\mathbf{A}}(t,u) + E\left[W_n^{\mathbf{A}_1,\mathbf{A}_2,\mathbf{A}}(t,u) \right]$ [31, Eq. (5)]. Similarly, this relation can be reduced to $E\left[W_{f+n}^{\mathbf{A}_1,\mathbf{A}}(t,u) \right] = W_f^{\mathbf{A}_1,\mathbf{A}}(t,u) + E\left[W_n^{\mathbf{A}_1,\mathbf{A}}(t,u) \right]$ for the ICFWD. Thus, the expectation-based output SNR of ICFWD is well-defined [36, 37]:

$$\text{ESNR}_{\text{ICFWD}}^{\mathbf{A}_1,\mathbf{A}} = \frac{\max\limits_{(t,u)\in\mathbb{R}^2} \left| W_f^{\mathbf{A}_1,\mathbf{A}}(t,u) \right|}{\underset{\underset{(t,u)}{\arg\max} \left| W_f^{\mathbf{A}_1,\mathbf{A}}(t,u) \right|}{\text{Mean}} \left\{ \left| E\left[W_n^{\mathbf{A}_1,\mathbf{A}}(t,u) \right] \right| \right\}}. \tag{7}$$

3.2 Inequality modeling of ICFWD

Since the value of the expectation-based output SNR of ICFWD depends only on the parameter matrices $\mathbf{A}_1, \mathbf{A}$ for given signals and noises, our latest work formulated an optimization model [37]

$$\max_{\mathbf{A}_1,\mathbf{A}} \text{ESNR}_{\text{ICFWD}}^{\mathbf{A}_1,\mathbf{A}}, \tag{8}$$

and then solved it to obtain the optimal LCT free parameters of ICFWD. However, it seems very complicated to solve the optimization model because there exists an inner optimization problem $\max\limits_{(t,u)\in\mathbb{R}^2} \left| W_f^{\mathbf{A}_1,\mathbf{A}}(t,u) \right|$ embedded in it. Indeed, our latest work demonstrated that the solution of the optimization model for multi-component LFM signals does not seem to be feasible because there are many absolute value terms found in the objective function need to be taken partial derivatives.

The inequality model is simpler than the optimization model due to no calculations for the inner optimization problem. Then, as an alternative to the expectation-based output SNR optimization model of ICFWD, the expectation-based output SNR inequality model between the ICFWD and WD might be suitable for the case of multi-component LFM signals.

Let the expectation-based output SNR of WD be [29], Eq. (33)]

Qiang *et al. EURASIP Journal on Advances in Signal Processing* (2021) 2021:122

Page 7 of 24

$$\mathrm{ESNR_{WD}} = \frac{\max\limits_{(t,\omega)\in\mathbb{R}^2}\left|\mathrm{W}_f(t,\omega)\right|}{\underset{\arg\max\limits_{(t,\omega)}\left|\mathrm{W}_f(t,\omega)\right|}{\mathrm{Mean}}\{|E[\mathrm{W}_n(t,\omega)]|\}}. \tag{9}$$

It is a constant for given signals and noises. Then, the value of the expectation-based output SNR of ICFWD can be larger than that of the expectation-based output SNR of WD for appropriate parameter matrices $\mathbf{A}_1, \mathbf{A}$. Thus, the expectation-based output SNR inequality model between the ICFWD and WD is well-established:

$$\mathrm{ESNR}_{\mathrm{ICFWD}}^{\mathbf{A}_1,\mathbf{A}} > \mathrm{ESNR}_{\mathrm{WD}}. \tag{10}$$

3.3 Inequality solving of ICFWD

The inequality (10) can be rewritten as

$$\frac{\max\limits_{(t,u)\in\mathbb{R}^2}\left|\mathrm{W}_f^{\mathbf{A}_1,\mathbf{A}}(t,u)\right|}{\underset{\arg\max\limits_{(t,u)}\left|\mathrm{W}_f^{\mathbf{A}_1,\mathbf{A}}(t,u)\right|}{\mathrm{Mean}}\left\{\left|E\left[\mathrm{W}_n^{\mathbf{A}_1,\mathbf{A}}(t,u)\right]\right|\right\}} > \frac{\max\limits_{(t,\omega)\in\mathbb{R}^2}\left|\mathrm{W}_f(t,\omega)\right|}{\underset{\arg\max\limits_{(t,\omega)}\left|\mathrm{W}_f(t,\omega)\right|}{\mathrm{Mean}}\{|E[\mathrm{W}_n(t,\omega)]|\}}. \tag{11}$$

There are two optimization problems $\max\limits_{(t,u)\in\mathbb{R}^2}\left|\mathrm{W}_f^{\mathbf{A}_1,\mathbf{A}}(t,u)\right|$ and $\max\limits_{(t,\omega)\in\mathbb{R}^2}\left|\mathrm{W}_f(t,\omega)\right|$ need to be solved firstly. It is clear that the solving methods are different for synthetic signals and real-world signals.

Synthetic signals. The ICFWD $\mathrm{W}_f^{\mathbf{A}_1,\mathbf{A}}(t,u)$ can be expressed as a function with the variables t, u and the parameters a_1, b_1, d_1, a, b, d. As for the WD $\mathrm{W}_f(t,\omega)$, it can be expressed as a function with the variables t, ω. Thanks to the classical extreme value theory [49], there is an analytic solution to the optimization problem $\max\limits_{(t,u)\in\mathbb{R}^2}\left|\mathrm{W}_f^{\mathbf{A}_1,\mathbf{A}}(t,u)\right|$, as well as the optimization problem $\max\limits_{(t,\omega)\in\mathbb{R}^2}\left|\mathrm{W}_f(t,\omega)\right|$. The former is an algebraic formulation with the parameters a_1, b_1, d_1, a, b, d, while the latter is an algebraic formulation without any parameters. Substituting them into (11) yields an algebraic inequality with the parameters a_1, b_1, d_1, a, b, d. In a word, the solution of the inequality model is an algebraic inequality for the case of synthetic signals.

Real-world signals. Due to peak detection algorithms [50], there is an arithmetic solution to the optimization problem $\max\limits_{(t,u)\in\mathbb{R}^2}\left|\mathrm{W}_f^{\mathbf{A}_1,\mathbf{A}}(t,u)\right|$ for given parameters a_1, b_1, d_1, a, b, d. Similarly, it follows an arithmetic solution to the optimization problem $\max\limits_{(t,\omega)\in\mathbb{R}^2}\left|\mathrm{W}_f(t,\omega)\right|$. Traversing all parameters and checking the inequality (11) gives a point set of parameters a_1, b_1, d_1, a, b, d. In order to narrow down the range of parameters traversal, the technique of uniform design [51] can be used to obtain a set of representative experimental points. In brief, the solution of the inequality model is a point set of parameters for the case of real-world signals.

4 Methods

This section focuses on solving the well-established inequality model for a kind of important synthetic signals, i.e., the LFM signals, including the single component and bi-component cases.

We first explore the solutions of the optimization problem $\max_{(t,u)\in\mathbb{R}^2}\left|W_f^{\mathbf{A}_1,\mathbf{A}}(t,u)\right|$ for single component and bi-component LFM signals respectively. We then obtain the solution of the mean problem $\underset{\arg\max_{(t,u)}\left|W_f^{\mathbf{A}_1,\mathbf{A}}(t,u)\right|}{\text{Mean}}\left\{\left|E\left[W_n^{\mathbf{A}_1,\mathbf{A}}(t,u)\right]\right|\right\}$ for zero-mean stationary noise. Finally, we formulate the solutions of the inequality model for single component and bi-component cases respectively.

4.1 ICFWD of single component LFM signal

This subsection revisits the optimization problem $\max_{(t,u)\in\mathbb{R}^2}\left|W_f^{\mathbf{A}_1,\mathbf{A}}(t,u)\right|$ for single component LFM signal given by

$$f(t) = e^{j\left(\alpha t + \beta t^2\right)}, \tag{12}$$

where the initial frequency α is arbitrary, and the frequency rate $\beta \neq 0$.

Let δ denote Dirac delta operator. Then, the amplitude of ICFWD of the single component LFM signal $f(t)$ can yield an impulse which is reproduced here as [27]

$$\sqrt{2\pi|bh_1|}\delta\left[u - b\left(\frac{d_1 - h_1}{2b_1} + \beta\right)t - \frac{\alpha}{2}b(h_1 + 1)\right], \tag{13}$$

where $h_1 = \frac{1}{2\beta b_1 + a_1}$. Here the LCT free parameters have to satisfy $2\beta b_1 + a_1 \neq 0$ and $\frac{a}{2b} + \frac{d_1 - h_1}{8b_1} - \frac{\beta}{4} = 0$.

As it is seen, the solution of the optimization problem reads [37]

$$\max_{(t,u)\in\mathbb{R}^2}\left|W_f^{\mathbf{A}_1,\mathbf{A}}(t,u)\right| = \sqrt{2\pi|bh_1|}. \tag{14}$$

4.2 ICFWD of bi-component LFM signal

This subsection studies the optimization problem $\max_{(t,u)\in\mathbb{R}^2}\left|W_f^{\mathbf{A}_1,\mathbf{A}}(t,u)\right|$ for bi-component LFM signal given by

$$f(t) = \widehat{g}(t) + \widetilde{g}(t) = e^{j\left(\widehat{\alpha}t + \widehat{\beta}t^2\right)} + e^{j\left(\widetilde{\alpha}t + \widetilde{\beta}t^2\right)}, \tag{15}$$

where $\widehat{\beta}, \widetilde{\beta} \neq 0$ and $\widehat{\beta} \neq \widetilde{\beta}$.

The bilinearity of the ICFWD implies that the ICFWD of the bi-component LFM signal $f(t)$ can be expanded as

$$W_{\widehat{g}}^{\mathbf{A}_1,\mathbf{A}}(t,u) + W_{\widetilde{g}}^{\mathbf{A}_1,\mathbf{A}}(t,u) + W_{\widehat{g},\widetilde{g}}^{\mathbf{A}_1,\mathbf{A}}(t,u) + W_{\widetilde{g},\widehat{g}}^{\mathbf{A}_1,\mathbf{A}}(t,u), \tag{16}$$

where $W_{\widehat{g}}^{\mathbf{A}_1,\mathbf{A}}(t,u)$ and $W_{\widetilde{g}}^{\mathbf{A}_1,\mathbf{A}}(t,u)$ are two auto terms, and

Qiang *et al. EURASIP Journal on Advances in Signal Processing*   (2021) 2021:122

Page 9 of 24

$$W^{\mathbf{A}_1,\mathbf{A}}_{\widehat{g},\widetilde{g}}(t,u) = \int_{-\infty}^{+\infty} \widehat{G}_{\mathbf{A}_1}\left(t + \frac{\pi}{2}\right)\widetilde{g}^*\left(t - \frac{\pi}{2}\right)\mathcal{K}_{\mathbf{A}}(u,\tau)\mathrm{d}\tau \tag{17}$$

and

$$W^{\mathbf{A}_1,\mathbf{A}}_{\widetilde{g},\widehat{g}}(t,u) = \int_{-\infty}^{+\infty} \widetilde{G}_{\mathbf{A}_1}\left(t + \frac{\pi}{2}\right)\widehat{g}^*\left(t - \frac{\pi}{2}\right)\mathcal{K}_{\mathbf{A}}(u,\tau)\mathrm{d}\tau \tag{18}$$

are two cross terms, and where $\widehat{G}_{\mathbf{A}_1}$ and $\widetilde{G}_{\mathbf{A}_1}$ denote the LCTs of $\widehat{g}$ and $\widetilde{g}$ relevant to the parameter matrix $\mathbf{A}_1$, respectively.

The amplitudes of the auto terms $W^{\mathbf{A}_1,\mathbf{A}}_{\widehat{g}}(t,u)$ and $W^{\mathbf{A}_1,\mathbf{A}}_{\widetilde{g}}(t,u)$ can generate impulses

$$\sqrt{2\pi\left|b\widehat{h}_1\right|}\delta\left[u - b\left(\frac{d_1 - \widehat{h}_1}{2b_1} + \widehat{\beta}\right)t - \frac{\widehat{\alpha}}{2}b\left(\widehat{h}_1 + 1\right)\right] \tag{19}$$

and

$$\sqrt{2\pi\left|b\widetilde{h}_1\right|}\delta\left[u - b\left(\frac{d_1 - \widetilde{h}_1}{2b_1} + \widetilde{\beta}\right)t - \frac{\widetilde{\alpha}}{2}b\left(\widetilde{h}_1 + 1\right)\right], \tag{20}$$

respectively, where $\widehat{h}_1 = \frac{1}{2\widehat{\beta}b_1+a_1}$ and $\widetilde{h}_1 = \frac{1}{2\widetilde{\beta}b_1+a_1}$, if and only if the LCT free parameters satisfy $2\widehat{\beta}b_1 + a_1 \neq 0$, $2\widetilde{\beta}b_1 + a_1 \neq 0$, $\frac{a}{2b} + \frac{d_1-\widehat{h}_1}{8b_1} - \frac{\widehat{\beta}}{4} = 0$, and $\frac{a}{2b} + \frac{d_1-\widetilde{h}_1}{8b_1} - \frac{\widetilde{\beta}}{4} = 0$.

Due to $\widehat{\beta} \neq \widetilde{\beta}$, $\frac{a}{2b} + \frac{d_1-\widehat{h}_1}{8b_1} - \frac{\widehat{\beta}}{4} = 0$, and $\frac{a}{2b} + \frac{d_1-\widetilde{h}_1}{8b_1} - \frac{\widetilde{\beta}}{4} = 0$, it follows that $\widetilde{\widehat{l}} \triangleq \frac{a}{2b} + \frac{d_1-\widetilde{h}_1}{8b_1} - \frac{\widehat{\beta}}{4} \neq 0$ and $\widehat{\widetilde{l}} \triangleq \frac{a}{2b} + \frac{d_1-\widehat{h}_1}{8b_1} - \frac{\widetilde{\beta}}{4} \neq 0$. Then, the cross terms $W^{\mathbf{A}_1,\mathbf{A}}_{\widehat{g},\widetilde{g}}(t,u)$ and $W^{\mathbf{A}_1,\mathbf{A}}_{\widetilde{g},\widehat{g}}(t,u)$ can not generate impulses because the amplitudes of them read

$$\sqrt{\frac{\left|\widehat{h}_1\right|}{2\left|b\widetilde{\widehat{l}}\right|}} \tag{21}$$

and

$$\sqrt{\frac{\left|\widetilde{h}_1\right|}{2\left|b\widehat{\widetilde{l}}\right|}}, \tag{22}$$

respectively. For the proof of the results, ones can refer to "Appendix 1".

Taking amplitude on each terms in (16), and substituting (19)–(22) gives

$$\sqrt{2\pi\left|b\widehat{h}_1\right|}\delta\left[u - b\left(\frac{d_1 - \widehat{h}_1}{2b_1} + \widehat{\beta}\right)t - \frac{\widehat{\alpha}}{2}b\left(\widehat{h}_1 + 1\right)\right]$$

$$+ \sqrt{2\pi\left|b\widetilde{h}_1\right|}\delta\left[u - b\left(\frac{d_1 - \widetilde{h}_1}{2b_1} + \widetilde{\beta}\right)t - \frac{\widetilde{\alpha}}{2}b\left(\widetilde{h}_1 + 1\right)\right] + \sqrt{\frac{\left|\widehat{h}_1\right|}{2\left|b\widetilde{\widehat{l}}\right|}} + \sqrt{\frac{\left|\widetilde{h}_1\right|}{2\left|b\widehat{\widetilde{l}}\right|}}.$$

$$\tag{23}$$

Thus, the solution of the optimization problem is

$$
\max_{(t,u)\in\mathbb{R}^2}\left|W_f^{\mathbf{A}_1,\mathbf{A}}(t,u)\right| = \sqrt{2\pi\left|b\widehat{h}_1\right|} + \sqrt{2\pi\left|b\widetilde{h}_1\right|}. \tag{24}
$$

4.3 ICFWD of zero-mean stationary noise

This subsection discusses the mean problem $\displaystyle\underset{\substack{\arg\max\\(t,u)}}{\mathrm{Mean}}\,\left\{\left|\mathrm{E}\left[W_n^{\mathbf{A}_1,\mathbf{A}}(t,u)\right]\right|\right\}$ for

zero-mean stationary noise.

The stationarity of the noise indicates that $\mathrm{E}[n(t_1)n^*(t_2)] = D\delta(t_1 - t_2)$, where D denotes the power spectral density of the noise. By using the sifting property of Delta function, the expectation of the ICFWD of the zero-mean stationary noise $n(t)$ can be calculated as

$$
\begin{aligned}
\mathrm{E}\left[W_n^{\mathbf{A}_1,\mathbf{A}}(t,u)\right] &= \iint_{-\infty}^{+\infty} \mathrm{E}\left[n(\varepsilon)n^*\left(t-\frac{\tau}{2}\right)\right]\mathcal{K}_{\mathbf{A}_1}\left(t+\frac{\tau}{2},\varepsilon\right)\mathcal{K}_{\mathbf{A}}(u,\tau)\mathrm{d}\varepsilon\mathrm{d}\tau \\
&= \frac{D}{2\pi\sqrt{jb_1}\sqrt{jb}}\mathrm{e}^{j\frac{d}{2b}u^2}\mathrm{e}^{j\frac{a_1+d_1-2}{2b_1}t^2}\int_{-\infty}^{+\infty}\mathrm{e}^{j\left(\frac{a_1+d_1+2}{8b_1}+\frac{a}{2b}\right)\tau^2}\mathrm{e}^{j\left(\frac{d_1-a_1}{2b_1}t-\frac{u}{b}\right)\tau}\mathrm{d}\tau.
\end{aligned} \tag{25}
$$

Owing to the well-known Gaussian integral formula [52]

$$
\int_{-\infty}^{+\infty}\mathrm{e}^{pt^2+qt}\mathrm{d}t = \sqrt{\frac{\pi}{-p}}\mathrm{e}^{-\frac{q^2}{4p}}\ (p\neq 0, \mathrm{Re}(p)\leq 0), \tag{26}
$$

the amplitude of $\mathrm{E}\left[W_n^{\mathbf{A}_1,\mathbf{A}}(t,u)\right]$ reads [37]

$$
D\sqrt{\frac{2}{\pi\left|b(a_1+d_1+2)+4ab_1\right|}} \tag{27}
$$

for $b(a_1+d_1+2)+4ab_1\neq 0$.

The noise is a uniform distribution in the time-frequency plane as $\left|\mathrm{E}\left[W_n^{\mathbf{A}_1,\mathbf{A}}(t,u)\right]\right|$ is independent of the variables t, u. Then, the solution of the mean problem takes

$$
\underset{\substack{\arg\max\\(t,u)}}{\mathrm{Mean}}\left\{\left|\mathrm{E}\left[W_n^{\mathbf{A}_1,\mathbf{A}}(t,u)\right]\right|\right\} = D\sqrt{\frac{2}{\pi\left|b(a_1+d_1+2)+4ab_1\right|}}. \tag{28}
$$

4.4 Solutions of the inequality model

This subsection deduces the solution of the inequality model for single component LFM signal added with zero-mean stationary noise. And on this basis, it obtains the solution of the inequality model for the bi-component case.

4.4.1 Single component case

Thanks to the equality $\frac{a}{2b} + \frac{d_1-h_1}{8b_1} - \frac{\beta}{4} = 0$, there is $b(a_1+d_1+2)+4ab_1 = b\frac{(h_1+1)^2}{h_1}$. See "Appendix 2" for the proof of this equation. Then, (28) can be simplified to [37]

$$\underset{\substack{\arg\max \left|W_f^{\mathbf{A_1,A}}(t,u)\right| \\ (t,u)}}{\text{Mean}} \left\{ \left| \mathrm{E}\left[W_n^{\mathbf{A_1,A}}(t,u) \right] \right| \right\} = \frac{D}{|h_1+1|} \sqrt{\frac{2}{\pi} \left| \frac{h_1}{b} \right|} \tag{29}$$

for $h_1 + 1 \neq 0$.

Substituting (14) and (29) into (7) gives the expectation-based output SNR of ICFWD for the single component case

$$\mathrm{ESNR}_{\mathrm{ICFWD}}^{\mathbf{A_1,A}} = \frac{\pi}{D} \left| b(h_1+1) \right|. \tag{30}$$

The expectation-based output SNR of WD for the single component case is reproduced here as [29, 30]

$$\mathrm{ESNR}_{\mathrm{WD}} = \frac{2\pi}{D}. \tag{31}$$

By substituting (30) and (31) into (10), it follows the solution of the inequality model for the single component case

$$\frac{\left| b(h_1+1) \right|}{2} > 1. \tag{32}$$

Note that this inequality implies $h_1 + 1 \neq 0$.

4.4.2 Bi-component case

Due to the continued equality $\frac{a}{2b} + \frac{d_1 - \widehat{h}_1}{8b_1} - \frac{\widehat{\beta}}{4} = \frac{a}{2b} + \frac{d_1 - \widetilde{h}_1}{8b_1} - \frac{\widetilde{\beta}}{4} = 0$, there is $b(a_1 + d_1 + 2) + 4ab_1 = b\frac{\left(\widehat{h}_1 + 1\right)^2}{\widehat{h}_1} = b\frac{\left(\widetilde{h}_1 + 1\right)^2}{\widetilde{h}_1}$. See "Appendix 2" for the proof of this continued equation. Then, (28) can be reduced to

$$\underset{\substack{\arg\max \left|W_f^{\mathbf{A_1,A}}(t,u)\right| \\ (t,u)}}{\text{Mean}} \left\{ \left| \mathrm{E}\left[W_n^{\mathbf{A_1,A}}(t,u) \right] \right| \right\} = \frac{D}{\left| \widehat{h}_1 + 1 \right|} \sqrt{\frac{2}{\pi} \left| \frac{\widehat{h}_1}{b} \right|} = \frac{D}{\left| \widetilde{h}_1 + 1 \right|} \sqrt{\frac{2}{\pi} \left| \frac{\widetilde{h}_1}{b} \right|} \tag{33}$$

for $\widehat{h}_1 + 1 \neq 0, \widetilde{h}_1 + 1 \neq 0$.

Substituting (24) and (33) into (7) yields the expectation-based output SNR of ICFWD for the bi-component case

$$
\begin{aligned}
\mathrm{ESNR}_{\mathrm{ICFWD}}^{\mathbf{A_1,A}} &= \frac{\sqrt{2\pi \left| b\widehat{h}_1 \right|}}{\underset{\substack{\arg\max \left|W_f^{\mathbf{A_1,A}}(t,u)\right| \\ (t,u)}}{\text{Mean}} \left\{ \left| \mathrm{E}\left[W_n^{\mathbf{A_1,A}}(t,u) \right] \right| \right\}} + \frac{\sqrt{2\pi \left| b\widetilde{h}_1 \right|}}{\underset{\substack{\arg\max \left|W_f^{\mathbf{A_1,A}}(t,u)\right| \\ (t,u)}}{\text{Mean}} \left\{ \left| \mathrm{E}\left[W_n^{\mathbf{A_1,A}}(t,u) \right] \right| \right\}} \\
&= \frac{\sqrt{2\pi \left| b\widehat{h}_1 \right|}}{\frac{D}{\left| \widehat{h}_1 + 1 \right|} \sqrt{\frac{2}{\pi} \left| \frac{\widehat{h}_1}{b} \right|}} + \frac{\sqrt{2\pi \left| b\widetilde{h}_1 \right|}}{\frac{D}{\left| \widetilde{h}_1 + 1 \right|} \sqrt{\frac{2}{\pi} \left| \frac{\widetilde{h}_1}{b} \right|}} \\
&= \frac{\pi}{D} \left[\left| b\left(\widehat{h}_1 + 1 \right) \right| + \left| b\left(\widetilde{h}_1 + 1 \right) \right| \right].
\end{aligned}
\tag{34}
$$

The expectation-based output SNR of WD for the bi-component case is reviewed as follows [29]:

$$\text{ESNR}_{\text{WD}} = \frac{4\pi}{D}. \tag{35}$$

By substituting (34) and (35) into (10), there is the solution of the inequality model for the bi-component case

$$\frac{\left|b\left(\widehat{h}_1 + 1\right)\right| + \left|b\left(\widetilde{h}_1 + 1\right)\right|}{4} > 1. \tag{36}$$

Here this inequality indicates $\widehat{h}_1 + 1 \neq 0, \widetilde{h}_1 + 1 \neq 0$.

See Table 2 for a summary of the solutions of the inequality model and the associated constraints on LCT free parameters.

5 Results and discussion

In order to demonstrate the usefulness and effectiveness of ICFWD in noisy LFM signals processing, this section designs some simulations to compare the detection accuracy of ICFWD, CICFWD, ACWD, KFWD, CRWD and WD, as well as the computing speed of ICFWD, CICFWD, ACWD, KFWD and CRWD.

The simulated single component and bi-component LFM signals $f_1(t)$ embedded in additive complex white Gaussian noise $n(t)$ are chosen as

$$f(t) = f_1(t) + n(t) = e^{j(t+0.5t^2)} + n(t) \tag{37}$$

and

$$f(t) = f_1(t) + n(t) = e^{j(0.5t+0.3t^2)} + e^{j(0.5t+0.6t^2)} + n(t), \tag{38}$$

respectively.

Assume that the observing interval is $[-5s, 5s]$, and the sampling frequency is 20 Hz for the single component case and 40 Hz for the bi-component case. Let the input SNR of the noisy signal $f(t)$ be $10\log_{10}\frac{\int_{-5}^{5}|f_1(t)|^2 dt}{\text{Var}[n(t)]}$, where the variance of the noise $\text{Var}[n(t)]$ equals to the product of the power spectral density of the noise and the bandwidth of the noise. In the simulations, the input SNR is assumed to be -10dB for the single component case and -8dB for the bi-component case.

Figure 1 compares the detection accuracy of ICFWD with that of CICFWD, ACWD, KFWD, CRWD and WD for the single component case. The ICFWD with LCT free

Table 2 Solutions of the inequality model for single component/bi-component LFM signal added with zero-mean stationary noise

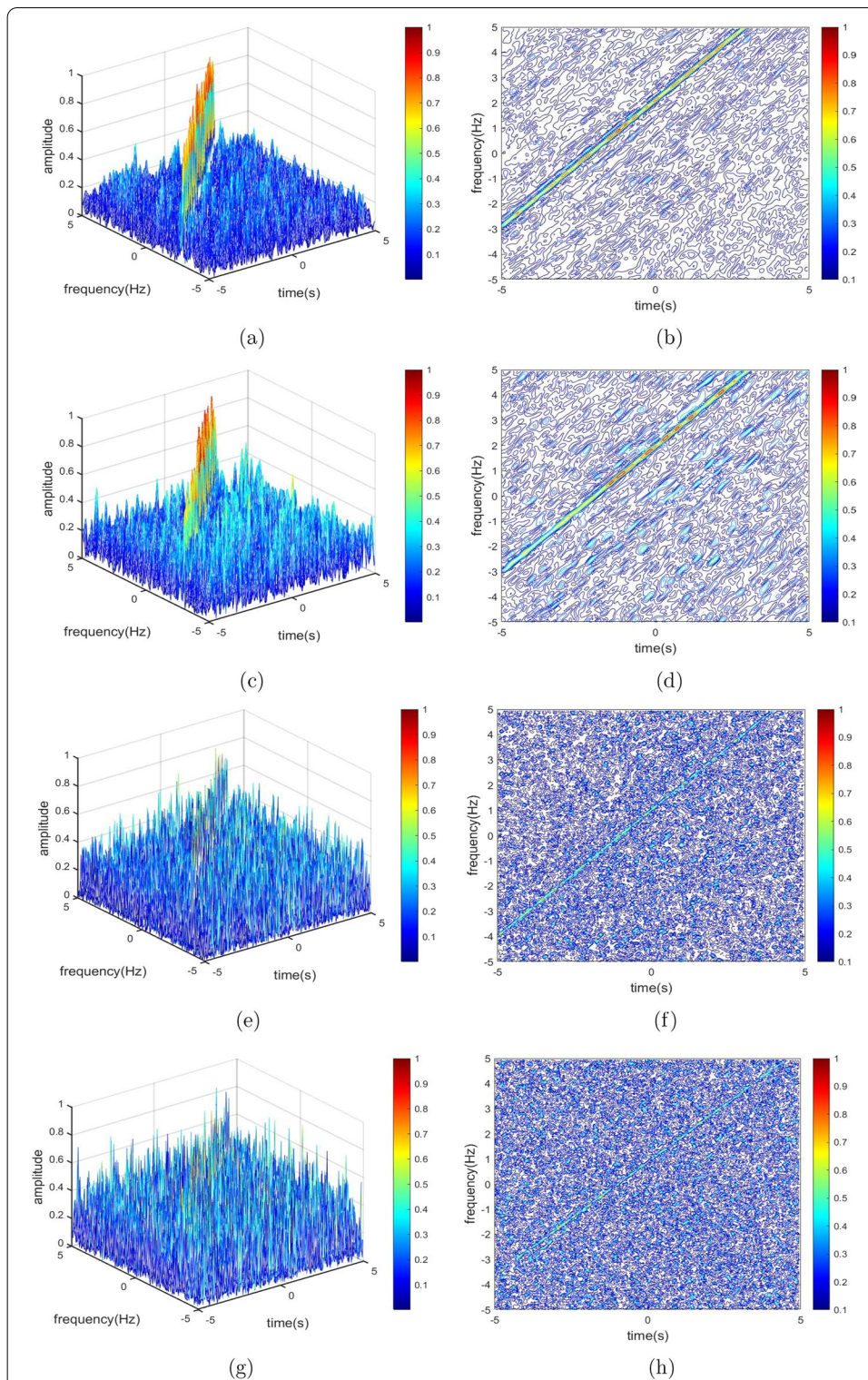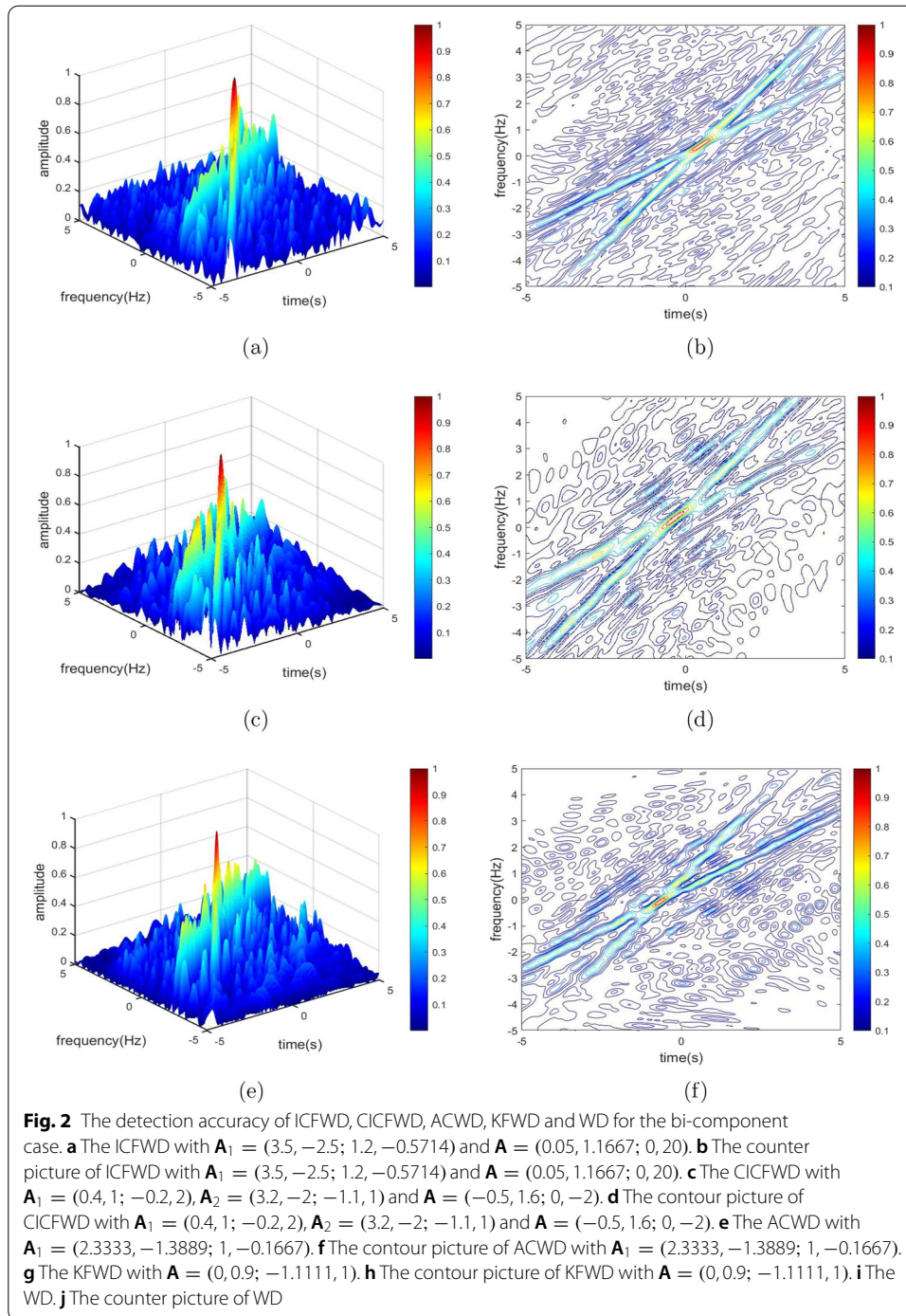|	Single component case	Bi-component case
Solutions of the model	$\frac{|b(h_1+1)|}{2} > 1$	$\frac{\left|b\left(\widehat{h}_1+1\right)\right|+\left|b\left(\widetilde{h}_1+1\right)\right|}{4} > 1$
Constraints on parameters	$2\beta b_1 + a_1 \neq 0,$	$2\widehat{\beta}b_1 + a_1 \neq 0, 2\widetilde{\beta}b_1 + a_1 \neq 0,$
	$\frac{a}{2b} + \frac{d_1-h_1}{8b_1} - \frac{\beta}{4} = 0$	$\frac{a}{2b} + \frac{d_1-\widehat{h}_1}{8b_1} - \frac{\widehat{\beta}}{4} = 0, \frac{a}{2b} + \frac{d_1-\widetilde{h}_1}{8b_1} - \frac{\widetilde{\beta}}{4} = 0$

Fig. 1 The detection accuracy of ICFWD, ClCFWD, ACWD, KFWD, CRWD and WD for the single component case. **a** The ICFWD with $\mathbf{A}_1 = (0.2111, 0.9; -0.9, 0.9)$ and $\mathbf{A} = (0.5, 2; 0, 2)$. **b** The counter picture of ICFWD with $\mathbf{A}_1 = (0.2111, 0.9; -0.9, 0.9)$ and $\mathbf{A} = (0.5, 2; 0, 2)$. **c** The ClCFWD with $\mathbf{A}_1 = (-1, 2; -0.5, 0)$, $\mathbf{A}_2 = (2, -1; 2, -0.5)$ and $\mathbf{A} = (1, 2; 0, 1)$. **d** The contour picture of ClCFWD with $\mathbf{A}_1 = (-1, 2; -0.5, 0)$, $\mathbf{A}_2 = (2, -1; 2, -0.5)$ and $\mathbf{A} = (1, 2; 0, 1)$. **e** The ACWD with $\mathbf{A}_1 = (0.5, 0.5; -0.5, 1.5)$. **f** The contour picture of ACWD with $\mathbf{A}_1 = (0.5, 0.5; -0.5, 1.5)$. **g** The KFWD with $\mathbf{A} = (0, 0.9; -1.1111, 1)$. **h** The contour picture of KFWD with $\mathbf{A} = (0, 0.9; -1.1111, 1)$. **i** The CRWD with $\mathbf{A}_1 = (1.4142, -1; -3, 2.8284)$. **j** The contour picture of CRWD with $\mathbf{A}_1 = (1.4142, -1; -3, 2.8284)$. **k** The WD. **l** The counter picture of WD
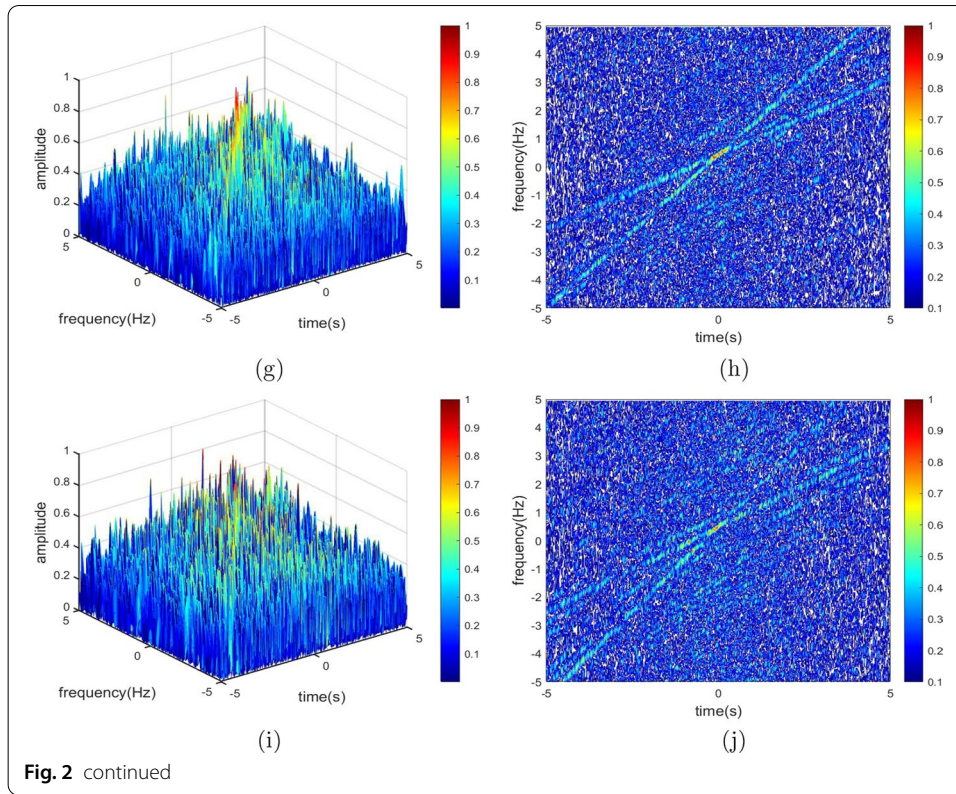
Fig. 1 continued
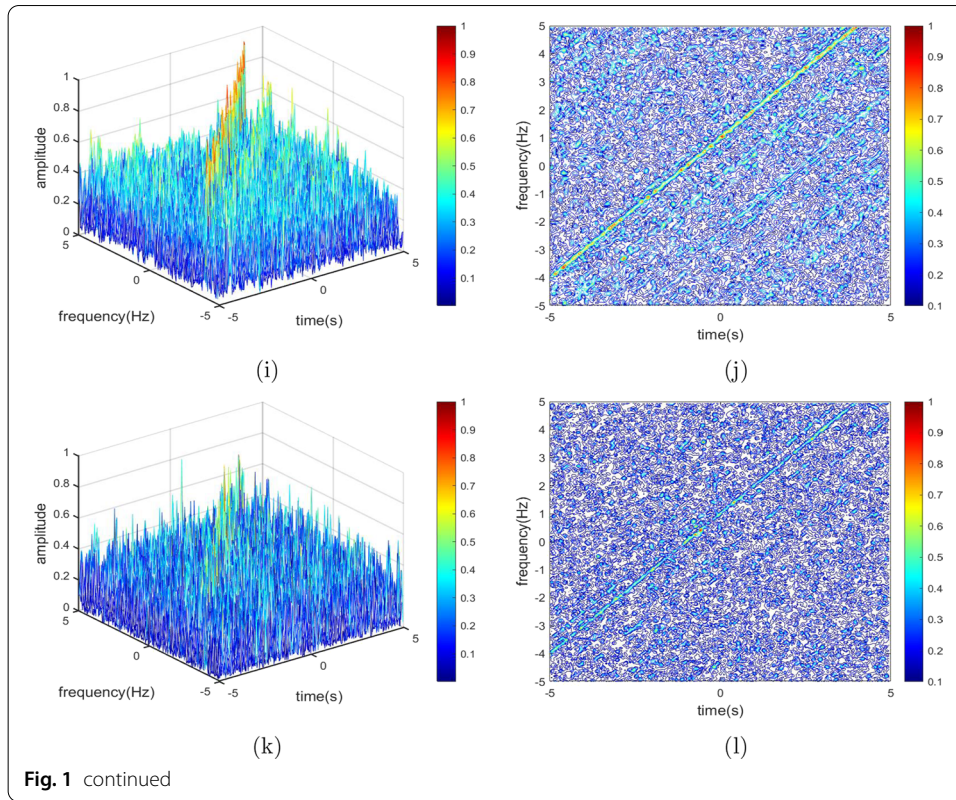
parameters satisfying $\frac{|b(h_1+1)|}{2} = 1.9 > 1, 2\beta b_1 + a_1 = 1.1111 \neq 0, \frac{a}{2b} + \frac{d_1 - h_1}{8b_1} - \frac{\beta}{4} = 0$ and the relevant contour picture are plotted in Fig. 1a, b, respectively. The CICFWD with LCT free parameters selected in [29] and the relevant contour picture are plotted in Fig. 1c, d, respectively. The ACWD with LCT free parameters selected in [2] and the relevant contour picture are plotted in Fig. 1e, f, respectively. The KFWD with LCT free parameters selected in [23] and the relevant contour picture are plotted in Fig. 1g, h, respectively. The CRWD with LCT free parameters selected in [26] and the relevant contour picture are plotted in Fig. 1i, j, respectively. The WD and the relevant contour picture are plotted in Fig. 1k, l, respectively.

Figure 2 compares the detection accuracy of ICFWD with that of CICFWD, ACWD, KFWD and WD for the bi-component case. The ICFWD with LCT free parameters satisfying $\frac{|b(\hat{h}_1+1)| + |b(\tilde{h}_1+1)|}{4} = 1.3125 > 1, 2\hat{\beta} b_1 + a_1 = 2 \neq 0, 2\tilde{\beta} b_1 + a_1 = 0.5 \neq 0,$ $\frac{a}{2b} + \frac{d_1 - \hat{h}_1}{8b_1} - \frac{\hat{\beta}}{4} = 0, \frac{a}{2b} + \frac{d_1 - \tilde{h}_1}{8b_1} - \frac{\tilde{\beta}}{4} = 0$ and the relevant contour picture are plotted in Fig. 2a, b, respectively. The CICFWD with LCT free parameters selected in [29] and the relevant contour picture are plotted in Fig. 2c, d, respectively. The ACWD with LCT free parameters selected in [2] and the relevant contour picture are plotted in Fig. 2e, f, respectively. The KFWD with LCT free parameters selected in [23] and the relevant contour picture are plotted in Fig. 2g, h, respectively. The WD and the relevant contour picture are plotted in Fig. 2i, j, respectively. It should be noted here that the CRWD fails to deal with general bi-component LFM signals unless the two components have opposite frequency rates [26].
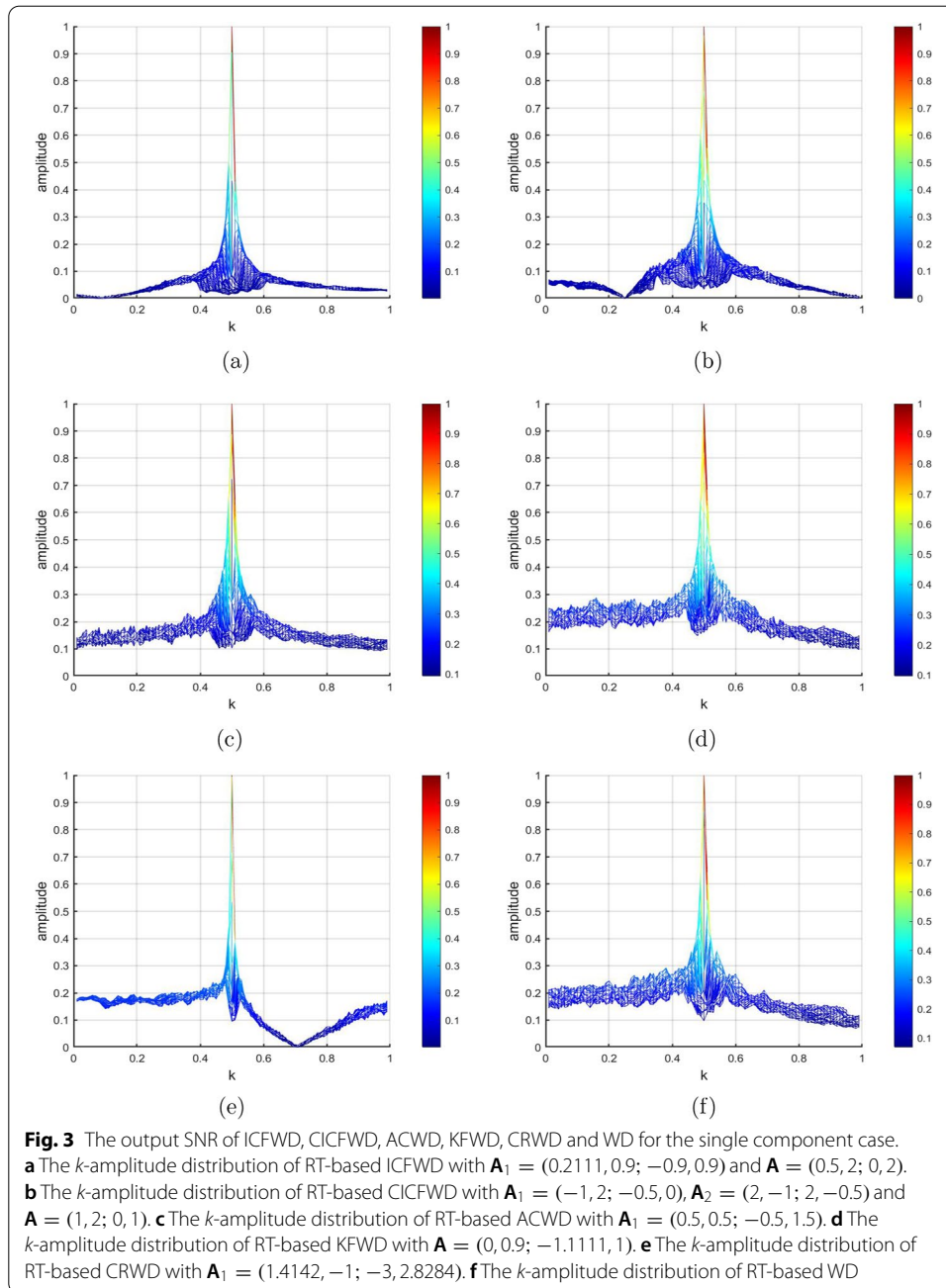
Fig. 2 The detection accuracy of ICFWD, CICFWD, ACWD, KFWD and WD for the bi-component case. **a** The ICFWD with $\mathbf{A}_1 = (3.5, -2.5; 1.2, -0.5714)$ and $\mathbf{A} = (0.05, 1.1667; 0, 20)$. **b** The counter picture of ICFWD with $\mathbf{A}_1 = (3.5, -2.5; 1.2, -0.5714)$ and $\mathbf{A} = (0.05, 1.1667; 0, 20)$. **c** The CICFWD with $\mathbf{A}_1 = (0.4, 1; -0.2, 2)$, $\mathbf{A}_2 = (3.2, -2; -1.1, 1)$ and $\mathbf{A} = (-0.5, 1.6; 0, -2)$. **d** The contour picture of CICFWD with $\mathbf{A}_1 = (0.4, 1; -0.2, 2)$, $\mathbf{A}_2 = (3.2, -2; -1.1, 1)$ and $\mathbf{A} = (-0.5, 1.6; 0, -2)$. **e** The ACWD with $\mathbf{A}_1 = (2.3333, -1.3889; 1, -0.1667)$. **f** The contour picture of ACWD with $\mathbf{A}_1 = (2.3333, -1.3889; 1, -0.1667)$. **g** The KFWD with $\mathbf{A} = (0, 0.9; -1.1111, 1)$. **h** The contour picture of KFWD with $\mathbf{A} = (0, 0.9; -1.1111, 1)$. **i** The WD. **j** The counter picture of WD

It can be observed from the sharpness of energy straight lines found in Figs. 1 and 2 that the ICFWD maintains the same level of detection accuracy as the CICFWD. Moreover, it achieves better detection accuracy than the ACWD, the KFWD, the CRWD, and the conventional WD.

It is well-known that the Radon transform (RT) [53] can accumulate energy straight lines, giving rise to the output SNR of time-frequency distributions which seems more

Fig. 2 continued

intuitive than the sharpness of energy straight lines. Figures 3 and 4 compare the output SNR of ICFWD with that of CICFWD, ACWD, KFWD, CRWD and WD for the single component case and the bi-component case, respectively. For the single component case, Fig. 3a plots the k-amplitude distribution of RT-based ICFWD [37] with LCT free parameters satisfying $\frac{|b(h_1+1)|}{2} = 1.9 > 1$, $2\beta b_1 + a_1 = 1.1111 \neq 0$, $\frac{a}{2b} + \frac{d_1-h_1}{8b_1} - \frac{\beta}{4} = 0$, Fig. 3b plots the k-amplitude distribution of RT-based CICFWD [29, 31] with LCT free parameters selected in [29], Fig. 3c plots the k-amplitude distribution of RT-based ACWD with LCT free parameters selected in [2], Fig. 3d plots the k-amplitude distribution of RT-based KFWD with LCT free parameters selected in [23], Fig. 3e plots the k-amplitude distribution of RT-based CRWD with LCT free parameters selected in [26], and Fig. 3f plots the k-amplitude distribution of RT-based WD [29, 31]. As for the bi-component case, Fig. 4a plots the k-amplitude distribution of RT-based ICFWD with LCT free parameters satisfying $\frac{|b(\widehat{h}_1+1)| + |b(\widetilde{h}_1+1)|}{4} = 1.3125 > 1$, $2\widehat{\beta} b_1 + a_1 = 2 \neq 0$, $2\widetilde{\beta} b_1 + a_1 = 0.5 \neq 0$, $\frac{a}{2b} + \frac{d_1-\widehat{h}_1}{8b_1} - \frac{\widehat{\beta}}{4} = 0$, $\frac{a}{2b} + \frac{d_1-\widetilde{h}_1}{8b_1} - \frac{\widetilde{\beta}}{4} = 0$, Fig. 4b plots the k-amplitude distribution of RT-based CICFWD with LCT free parameters selected in [29], Fig. 4c plots the k-amplitude distribution of RT-based ACWD with LCT free parameters selected in [2], Fig. 4d plots the k-amplitude distribution of RT-based KFWD with LCT free parameters selected in [23], and Fig. 4e plots the k-amplitude distribution of RT-based WD.

Fig. 3 The output SNR of ICFWD, CICFWD, ACWD, KFWD, CRWD and WD for the single component case. **a** The k-amplitude distribution of RT-based ICFWD with $\mathbf{A}_1 = (0.2111, 0.9; -0.9, 0.9)$ and $\mathbf{A} = (0.5, 2; 0, 2)$. **b** The k-amplitude distribution of RT-based CICFWD with $\mathbf{A}_1 = (-1, 2; -0.5, 0)$, $\mathbf{A}_2 = (2, -1; 2, -0.5)$ and $\mathbf{A} = (1, 2; 0, 1)$. **c** The k-amplitude distribution of RT-based ACWD with $\mathbf{A}_1 = (0.5, 0.5; -0.5, 1.5)$. **d** The k-amplitude distribution of RT-based KFWD with $\mathbf{A} = (0, 0.9; -1.1111, 1)$. **e** The k-amplitude distribution of RT-based CRWD with $\mathbf{A}_1 = (1.4142, -1; -3, 2.8284)$. **f** The k-amplitude distribution of RT-based WD

It is obvious from the amplitude of noises found in Figs. 3 and 4 that the ICFWD maintains the same level of output SNR as the CICFWD. Moreover, it achieves higher output SNR than the ACWD, the KFWD, the CRWD, and the conventional WD.

Tables 3 and 4 record the computing time of ICFWD, CICFWD, ACWD, KFWD and CRWD in four different sampling frequencies 20 Hz, 40 Hz, 80 Hz and 120 Hz by using MATLAB language (version R2021a) and Desktop equipped with Intel(R) Core(TM)i5-9400F CPU @ 2.90 GHz for the single component case and the bi-component case, respectively. The computing time is statistically obtained by averaging

Fig. 4 The output SNR of ICFWD, CICFWD, ACWD, KFWD and WD for the bi-component case. **a** The k-amplitude distribution of RT-based ICFWD with $\mathbf{A}_1 = (3.5, -2.5; 1.2, -0.5714)$ and $\mathbf{A} = (0.05, 1.1667; 0, 20)$. **b** The k-amplitude distribution of RT-based CICFWD with $\mathbf{A}_1 = (0.4, 1; -0.2, 2)$, $\mathbf{A}_2 = (3.2, -2; -1.1, 1)$ and $\mathbf{A} = (-0.5, 1.6; 0, -2)$. **c** The k-amplitude distribution of RT-based ACWD with $\mathbf{A}_1 = (2.3333, -1.3889; 1, -0.1667)$. **d** The k-amplitude distribution of RT-based KFWD with $\mathbf{A} = (0, 0.9; -1.1111, 1)$. **e** The k-amplitude distribution of RT-based WD

Table 3 Computing time of ICFWD, CICFWD, ACWD, KFWD and CRWD in sampling frequencies 20 Hz, 40 Hz, 80 Hz and 120 Hz for the single component case

Sampling frequency (Hz)	Computing time (s)				
	ICFWD	**CICFWD**	**ACWD**	**KFWD**	**CRWD**
20	0.0190	0.0274	0.0190	0.0104	0.0285
40	0.0557	0.0775	0.0563	0.0331	0.0792
80	0.1930	0.2595	0.1967	0.1272	0.2666
120	0.4559	0.5919	0.4674	0.3335	0.6035

Table 4 Computing time of ICFWD, CICFWD, ACWD and KFWD in sampling frequencies 20 Hz, 40 Hz, 80 Hz and 120 Hz for the bi-component case

Sampling frequency (Hz)	Computing time (s)			
	ICFWD	CICFWD	ACWD	KFWD
20	0.0190	0.0275	0.0196	0.0102
40	0.0560	0.0788	0.0576	0.0332
80	0.1958	0.2632	0.2031	0.1274
120	0.4718	0.5978	0.4679	0.3330
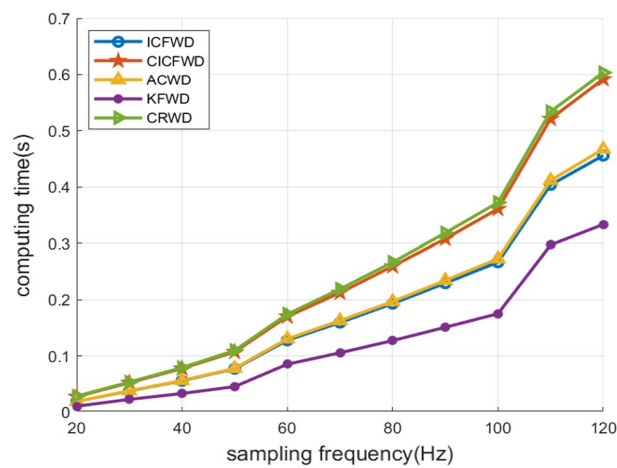
Fig. 5 The computing speed of ICFWD, CICFWD, ACWD, KFWD and CRWD for the single component case
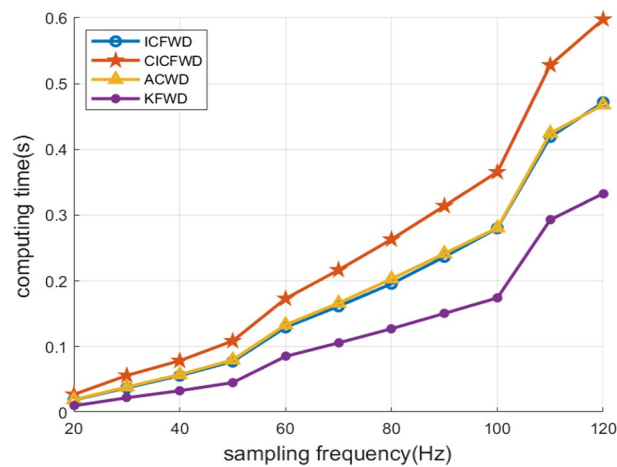
Fig. 6 The computing speed of ICFWD, CICFWD, ACWD and KFWD for the bi-component case

over 1000 realizations. Figures 5 and 6 plot a comparison of the computing speed of ICFWD, CICFWD, ACWD, KFWD and CRWD for the single component case and the bi-component case, respectively.

As it is seen, the ICFWD maintains the same level of computation efficiency as the ACWD. Moreover, it exhibits higher computation efficiency than the CICFWD and CRWD while lower computation efficiency than the KFWD.

6 Conclusion

Since the ICFWD has a significant benefit in the tradeoff between detection accuracy and computational complexity among all of the linear canonical domain WDs, the application of ICFWD in weak multi-component LFM signals detection problem has been investigated. By modeling and solving the expectation-based output SNR inequality between the ICFWD and WD, the selecting methods of the LCT free parameters of the ICFWD for both the single component and bi-component cases are derived. A larger number of numerical experiments demonstrate the correctness of theoretical results. It turns out that the detection accuracy of ICFWD is similar to that of CICFWD, and it is better than the detection accuracy of ACWD, KFWD, CRWD and the conventional WD. In addition, the ICFWD has computation efficiency comparable to the ACWD, and it is superior to the CICFWD and CRWD in high computation efficiency while inferior to the KFWD.

Appendix 1: Derivation of the cross terms $W_{\widehat{g},\widetilde{g}}^{\mathbf{A}_1,\mathbf{A}}(t,u)$ and $W_{\widetilde{g},\widehat{g}}^{\mathbf{A}_1,\mathbf{A}}(t,u)$

The cross term $W_{\widehat{g},\widetilde{g}}^{\mathbf{A}_1,\mathbf{A}}(t,u)$ is revisited as follows:

$$W_{\widehat{g},\widetilde{g}}^{\mathbf{A}_1,\mathbf{A}}(t,u) = \int_{-\infty}^{+\infty} \widehat{G}_{\mathbf{A}_1}\left(t + \frac{\pi}{2}\right)\widetilde{g}^*\left(t - \frac{\pi}{2}\right)\mathcal{K}_{\mathbf{A}}(u,\tau)\mathrm{d}\tau, \tag{39}$$

where

$$\widehat{G}_{\mathbf{A}_1}\left(t + \frac{\pi}{2}\right) = \int_{-\infty}^{+\infty} \widehat{g}(\rho)\mathcal{K}_{\mathbf{A}_1}\left(t + \frac{\pi}{2}, \rho\right)\mathrm{d}\rho. \tag{40}$$

Thanks to (26), substituting $\widehat{g}(t) = \mathrm{e}^{\mathrm{j}\left(\widehat{\alpha}t + \widehat{\beta}t^2\right)}$ and $\widetilde{g}(t) = \mathrm{e}^{\mathrm{j}\left(\widetilde{\alpha}t + \widetilde{\beta}t^2\right)}$ into (39) gives

$$\left|W_{\widehat{g},\widetilde{g}}^{\mathbf{A}_1,\mathbf{A}}(t,u)\right| = \sqrt{\frac{\left|\widehat{h}_1\right|}{2\pi|b|}}\left|\int_{-\infty}^{+\infty} \mathrm{e}^{\mathrm{j}\left(\frac{a}{2b} + \frac{d_1 - \widehat{h}_1}{8b_1} - \frac{\widetilde{\beta}}{4}\right)\tau^2}\mathrm{e}^{-\mathrm{j}\left[\frac{u}{b} - \left(\frac{d_1 - \widehat{h}_1}{2b_1} + \widetilde{\beta}\right)t - \frac{\widehat{\alpha}}{2}\left(\widehat{h}_1 + 1\right)\right]\tau}\mathrm{d}\tau\right| \tag{41}$$

for $\frac{1}{\widehat{h}_1} = 2\widehat{\beta}b_1 + a_1 \neq 0$, and subsequently, there is

$$\left|W_{\widehat{g},\widetilde{g}}^{\mathbf{A}_1,\mathbf{A}}(t,u)\right| = \sqrt{\frac{\left|\widehat{h}_1\right|}{2\left|b\widetilde{\widetilde{l}}\right|}} \tag{42}$$

for $\widetilde{\widetilde{l}} = \frac{a}{2b} + \frac{d_1 - \widehat{h}_1}{8b_1} - \frac{\widetilde{\beta}}{4} \neq 0$.

Similarly, it follows that

Qiang *et al. EURASIP Journal on Advances in Signal Processing* (2021) 2021:122

Page 21 of 24

$$\left| W_{\tilde{g},\hat{g}}^{\mathbf{A}_1,\mathbf{A}}(t,u) \right| = \sqrt{\frac{\left| \overline{\widetilde{h}_1} \right|}{2 \left| \overline{\widehat{bl}} \right|}} \tag{43}$$

for $\frac{1}{\overline{\widetilde{h}_1}} = 2\widetilde{\beta}b_1 + a_1 \neq 0$ and $\overline{\widehat{l}} \triangleq \frac{a}{2b} + \frac{d_1 - \widetilde{h}_1}{8b_1} - \frac{\widehat{\beta}}{4} \neq 0.$

Appendix 2: Derivation of the equations $b(a_1 + d_1 + 2) + 4ab_1 = b\frac{(h_1+1)^2}{h_1}$ and $b(a_1 + d_1 + 2) + 4ab_1 = b\frac{\left(\widehat{h}_1+1\right)^2}{\widehat{h}_1} = b\frac{\left(\widetilde{h}_1+1\right)^2}{\widetilde{h}_1}$

From the equality

$$\frac{a}{2b} + \frac{d_1 - h_1}{8b_1} - \frac{\beta}{4} = 0, \tag{44}$$

there is

$$a = \left(\frac{\beta}{2} - \frac{d_1 - h_1}{4b_1} \right) b. \tag{45}$$

Substituting into $b(a_1 + d_1 + 2) + 4ab_1$ gives

$$b(a_1 + d_1 + 2) + 4ab_1 = b(2\beta b_1 + a_1 + h_1 + 2), \tag{46}$$

and then it follows that

$$\begin{aligned} b(a_1 + d_1 + 2) + 4ab_1 &= b\left(\frac{1}{h_1} + h_1 + 2 \right) \\ &= b\frac{(h_1 + 1)^2}{h_1} \end{aligned} \tag{47}$$

because of $2\beta b_1 + a_1 = \frac{1}{h_1}$.

Similarly, from the continued equality $\frac{a}{2b} + \frac{d_1 - \widehat{h}_1}{8b_1} - \frac{\widehat{\beta}}{4} = \frac{a}{2b} + \frac{d_1 - \widetilde{h}_1}{8b_1} - \frac{\widetilde{\beta}}{4} = 0$, and $2\widehat{\beta}b_1 + a_1 = \frac{1}{\widehat{h}_1}$ and $2\widetilde{\beta}b_1 + a_1 = \frac{1}{\widetilde{h}_1}$, there are two equations

$$b(a_1 + d_1 + 2) + 4ab_1 = b\frac{\left(\widehat{h}_1 + 1\right)^2}{\widehat{h}_1} \tag{48}$$

and

$$b(a_1 + d_1 + 2) + 4ab_1 = b\frac{\left(\widetilde{h}_1 + 1\right)^2}{\widetilde{h}_1}. \tag{49}$$

Abbreviations

LCT: Linear canonical transform; FT: Fourier transform; FRFT: Fractional Fourier transform; WD: Wigner distribution; ICF: Instantaneous cross-correlation function; CICF: Closed-form instantaneous cross-correlation function; ACWD: Affine characteristic Wigner distribution; KFWD: Kernel function Wigner distribution; CRWD: Convolution representation Wigner distribution; ICFWD: ICF type of Wigner distribution; CICFWD: CICF type of Wigner distribution; SNR: Signal-to-noise ratio; LFM: Linear frequency-modulated; RT: Radon transform.

Authors' contributions

The inequality model proposed in this paper has been conceived by S-ZQ and Z-CZ, S-ZQ, XJ, X-YS, A-YW, and YS made the theoretical analysis and numerical experiments. S-ZQ, XJ, P-YH, and Z-CZ wrote the initial draft. S-ZQ and Z-CZ edited the revised version. Z-CZ, Y-JC, XJ, and S-ZQ contributed to the funding support. The authors read and approved the final manuscript.

Authors' informations

Sheng-Zhou Qiang was born in Wuxi City, Jiangsu Province, China, in 2001. He is currently studying as a third-year undergraduate in Information and Computing Sciences with the School of Mathematics and Statistics, Nanjing University of Information Science and Technology, Nanjing, Jiangsu, China.

Xian Jiang was born in Changzhou City, Jiangsu Province, China, in 2000. He is currently studying as a third-year undergraduate in Information and Computing Sciences with the School of Mathematics and Statistics, Nanjing University of Information Science and Technology, Nanjing, Jiangsu, China.

Pu-Yu Han was born in Shenyang City, Liaoning Province, China, in 2001. He is currently studying as a third-year undergraduate in Information and Computing Sciences with the School of Mathematics and Statistics, Nanjing University of Information Science and Technology, Nanjing, Jiangsu, China.

Xi-Ya Shi was born in Pizhou City, Jiangsu Province, China, in 1998. She received a double B.S. degree in Financial Mathematics and Economic Law from Yancheng Normal University, Yancheng, Jiangsu, China, in 2020. She is currently working towards the M.S. degree in Mathematics with the School of Mathematics and Statistics, Nanjing University of Information Science and Technology, Nanjing, Jiangsu, China.

An-Yang Wu was born in Nanjing, Jiangsu Province, China, in 1997. He received the B.S. degree in Applied Statistics from Nanjing University of Information Science and Technology, Nanjing, Jiangsu, China, in 2019. He is currently working towards the M.S. degree in Mathematics with the School of Mathematics and Statistics, Nanjing University of Information Science and Technology, Nanjing, Jiangsu, China.

Yun Sun was born in Nantong City, Jiangsu Province, China, in 2001. She is currently studying as a third-year undergraduate in Information and Computing Sciences with the School of Mathematics and Statistics, Nanjing University of Information Science and Technology, Nanjing, Jiangsu, China.

Yun-Jie Chen was born in Yancheng city, Jiangsu, China, in 1980. He received the Ph.D. degree in pattern recognition and intelligent system from the Nanjing University of Science and Technology, Nanjing, China, in 2008. He is currently a Full Professor with the School of Mathematics and Statistics, NUIST, Nanjing. His research interests are mainly focused on pattern recognition, image segmentation, and image processing.

Zhi-Chao Zhang was born in Jingdezhen City, Jiangxi Province, China, in 1991. He received the B.S. degree in Mathematics and Applied Mathematics from Gannan Normal University, Ganzhou, Jiangxi, China, in 2012, and the Ph.D. degree in Mathematics of Uncertainty Processing from Sichuan University, Chengdu, Sichuan, China, in 2018. From September 2017 to September 2018, he was awarded a grant from the China Scholarship Council to study as a visiting student researcher with the Department of Electrical and Computer Engineering, Tandon School of Engineering, New York University, Brooklyn, NY, USA. Since 2019, he has been with the School of Mathematics and Statistics, Nanjing University of Information Science and Technology, Nanjing, Jiangsu, China, where he is currently a Full Professor and Master's Supervisor. He is currently working as the Macau Young Scholars Postdoctoral Fellow in Information and Communication Engineering with the Faculty of Information Technology, Macau University of Science and Technology, Macau, China. His research interests cover the mathematical theories, methods and applications in signal and information processing, including fundamental theories such as Fourier analysis, functional analysis and harmonic analysis, applied theories such as signal representation, sampling, reconstruction, filter, separation, detection and estimation, and engineering technologies such as satellite communications, radar detection and electronic countermeasures.

Availability of data and materials

Please contact the authors for data requests.

Declarations

Consent for publication

This research does not contain any individual person's data in any form (including individual details, images, or videos).

Qiang *et al. EURASIP Journal on Advances in Signal Processing*   (2021) 2021:122

Page 23 of 24

Author details
[1]School of Mathematics and Statistics, Nanjing University of Information Science and Technology, Nanjing 210044, China.
[2]Faculty of Information Technology, Macau University of Science and Technology, Macau 999078, China.

References
1. A. Yelashetty, N. Gupta, D. Dhirhe, U. Gopinathan, Linear canonical transform as a tool to analyze coherence proper-ties of electromagnetic beams propagating in a quadratic phase system. J. Opt. Soc. Am. A **37**(8), 1350–1360 (2020)
2. S.C. Pei, J.J. Ding, Relations between fractional operations and time-frequency distributions and their applications. IEEE Trans. Signal Process. **49**(8), 1638–1655 (2001)
3. A. Stern, Sampling of linear canonical transformed signals. Signal Process. **86**(7), 1421–1425 (2006)
4. R.N. Bracewell, *The Fourier Transform and Its Applications* (McGraw-Hill, Boston, 2000)
5. H.M. Ozaktas, M.A. Kutay, Z. Zalevsky, *The Fractional Fourier Transform With Applications in Optics and Signal Processing* (Wiley, New York, 2001)
6. R. Tao, B. Deng, Y. Wang, *Fractional Fourier Transform and Its Applications* (Tisinghua University Press, Beijing, 2009)
7. J. Shi, Y.N. Zhao, W. Xiang, V. Monga, X.P. Liu, R. Tao, Deep scattering network with fractional wavelet transform. IEEE Trans. Signal Process. **69**, 4740–4757 (2021)
8. C. Gao, R. Tao, X.J. Kang, Weak target detection in the presence of sea clutter using Radon-fractional Fourier trans-form canceller. IEEE J. Sel. Topics Appl. Earth Observ. Remote Sens. **14**, 5818–5830 (2021)
9. Y. Liu, F. Zhang, H.X. Miao, R. Tao, The hopping discrete fractional Fourier transform. Signal Process. **178**, 107763 (2021)
10. H. Oberst, D. Kouznetsov, K. Shimizu, J.-I. Fujita, F. Shimizu, Fresnel diffraction mirror for an atomic wave. Phys. Rev. Lett. **94**, 013203 (2005)
11. S. Abe, J.T. Sheridan, Optical operations on wave functions as the Abelian subgroups of the special affine Fourier transformation. Opt. Lett. **19**(22), 1801–1803 (1994)
12. K. İmre, E. Özizmir, Wigner method in quantum statistical mechanics. J. Math. Phys. **8**(5), 1097–1108 (1967)
13. B. Boashash, Note on the use of the Wigner distribution for time-frequency signal analysis. IEEE Trans. Acoust. Speech Signal Process. **36**(9), 1518–1521 (1988)
14. P. Gonçalvès, R.G. Baraniuk, Pseudo affine Wigner distributions: definition and kernel formulation. IEEE Trans. Signal Process. **46**(6), 1505–1516 (1998)
15. W. Martin, P. Flandrin, Wigner–Ville spectral analysis of nonstationary processes. IEEE Trans. Acoust. Speech Signal Process. **33**(6), 1461–1470 (1985)
16. L. Stanković, A method for time-frequency analysis. IEEE Trans. Signal Process. **42**(1), 225–229 (1994)
17. L.J. Stanković, S. Stanković, An analysis of instantaneous frequency representation using time-frequency distribu-tions-generalized Wigner distribution. IEEE Trans. Signal Process. **43**(2), 549–552 (1995)
18. B. Boashash, P. O'Shea, Polynomial Wigner–Ville distributions and their relationship to time-varying higher order spectra. IEEE Trans. Signal Process. **42**(1), 216–220 (1994)
19. H.I. Choi, W.J. Williams, Improved time-frequency representation of multicomponent signals using exponential kernels. IEEE Trans. Acoust. Speech Signal Process. **37**(6), 862–871 (1989)
20. Z.C. Zhang, X. Jiang, S.Z. Qiang, A. Sun, Z.Y. Liang, X.Y. Shi, A.Y. Wu, Scaled Wigner distribution using fractional instan-taneous autocorrelation. Optik **237**, 166691 (2021)
21. T. Thayaparan, J. Marchioni, A. Kelsall, R. Riddolls, Improved frequency monitoring system for sky-wave over-the-horizon radar in Canada. IEEE Geosci. Remote. Sens. Lett. **17**(4), 606–610 (2020)
22. F.B. Duan, F. Chapeau-Blondeau, D. Abbott, Weak signal detection: condition for noise induced enhancement. Digit. Signal Process. **23**(5), 1585–1591 (2013)
23. R.F. Bai, B.Z. Li, Q.Y. Cheng, Wigner–Ville distribution associated with the linear canonical transform. J. Appl. Math. **2012**, 740161 (2012)
24. T.W. Che, B.Z. Li, T.Z. Xu, The ambiguity function associated with the linear canonical transform. EURASIP J. Adv. Signal Process. **2012**, 138 (2012)
25. R. Tao, Y.E. Song, Z.J. Wang, Y. Wang, Ambiguity function based on the linear canonical transform. IET Signal Process. **6**(6), 568–576 (2012)
26. Z.C. Zhang, New Wigner distribution and ambiguity function based on the generalized translation in the linear canonical transform domain. Signal Process. **118**, 51–61 (2016)
27. Z.C. Zhang, Unified Wigner–Ville distribution and ambiguity function in the linear canonical transform domain. Signal Process. **114**, 45–60 (2015)
28. Z.C. Zhang, M.K. Luo, New integral transforms for generalizing the Wigner distribution and ambiguity function. IEEE Signal Process. Lett. **22**(4), 460–464 (2015)
29. Z.C. Zhang, Linear canonical Wigner distribution based noisy LFM signals detection through the output SNR improvement analysis. IEEE Trans. Signal Process. **67**(21), 5527–5542 (2019)
30. Z.C. Zhang, S.Z. Qiang, X. Jiang, P.Y. Han, X.Y. Shi, A.Y. Wu, Linear canonical Wigner distribution of noisy LFM signals via variance-SNR based inequalities system analysis. Optik **237**, 166712 (2021)
31. Z.C. Zhang, The optimal linear canonical Wigner distribution of noisy linear frequency-modulated signals. IEEE Signal Process. Lett. **26**(8), 1127–1131 (2019)

Qiang *et al. EURASIP Journal on Advances in Signal Processing*   (2021) 2021:122

Page 24 of 24

32. Z.C. Zhang, D. Li, Y.J. Chen, J.W. Zhang, Linear canonical Wigner distribution of noisy LFM signals via multiobjective optimization analysis involving variance-SNR. IEEE Commun. Lett. **25**(2), 546–550 (2021)
33. D.M.J. Cowell, S. Freear, Separation of overlapping linear frequency modulated (LFM) signals using the fractional fourier transform. IEEE Trans. Ultrason. Ferroelectr. Freq. Control **57**(10), 2324–2333 (2020)
34. M.A.B. Othman, J. Belz, B. Farhang-Boroujeny, Performance analysis of matched filter bank for detection of linear frequency modulated chirp signals. IEEE Trans. Aerosp. Electron. Syst. **53**(1), 41–54 (2017)
35. X.Y. Peng, Y. Zhang, W. Wang, S.Q. Yang, Broadband mismatch calibration for time-interleaved ADC based on linear frequency modulated signal. IEEE Trans. Circ. Syst. I Reg. Pap. **68**(9), 3621–3630 (2021)
36. X.Y. Shi, A.Y. Wu, Y.Sun, S.Z. Qiang, X. Jiang, P.Y. Han, Y.J. Chen, Z.C. Zhang, Unique parameters selection strategy of linear canonical Wigner distribution via multiobjective optimization modeling (Submitted)
37. A.Y. Wu, X.Y. Shi, Y. Sun, X. Jiang, S.Z. Qiang, P.Y. Han, Z.C. Zhang, A computationally efficient optimal Wigner distribution in LCT domains for detecting noisy LFM signals (Submitted)
38. D.P. Bertsekas, *Constrained Optimization and Lagrange Multiplier Methods* (Academic, New York, 1982)
39. S.A. Collins, Lens-system diffraction integral written in terms of matrix optics. J. Opt. Soc. Am. **60**(9), 1168–1177 (1970)
40. M. Moshinsky, C. Quesne, Linear canonical transformations and their unitary representations. J. Math. Phys. **12**(8), 1772–1783 (1971)
41. J.J. Healy, M.A. Kutay, H.M. Ozaktas, J.T. Sheridan (eds.), *Linear Canonical Transforms: Theory and Applications* (Springer, New York, 2016)
42. T.Z. Xu, B.Z. Li, *Linear Canonical Transforms and Its Applications* (Science Press, Beijing, 2013)
43. J. Shi, X.P. Liu, Y.N. Zhao, S. Shi, X.J. Sha, Q.Y. Zhang, Filter design for constrained signal reconstruction in linear canonical transform domain. IEEE Trans. Signal Process. **66**(24), 6534–6548 (2018)
44. J. Shi, X.P. Liu, F.G. Yan, W.B. Song, Error analysis of reconstruction from linear canonical transform based sampling. IEEE Trans. Signal Process. **66**(7), 1748–1760 (2018)
45. D.Y. Wei, Y.M. Li, Convolution and multichannel sampling for the offset linear canonical transform and their applications. IEEE Trans. Signal Process. **67**(23), 6009–6024 (2019)
46. D.Y. Wei, H.M. Hu, Theory and applications of short-time linear canonical transform. Digit. Signal Process. (In Press)
47. Q. Feng, B.Z. Li, J.M. Rassias, Weighted Heisenberg-Pauli-Weyl uncertainty principles for the linear canonical transform. Signal Process. **165**, 209–221 (2019)
48. W.B. Gao, B.Z. Li, Uncertainty principles for the short-time linear canonical transform of complex signals. Digit. Signal Process. **111**, 102953 (2021)
49. L. de Haan, A. Ferreira, *Extreme Value Theory: An Introduction* (Springer Science+Business Media LLC, New York, 2006)
50. T. Maka, Influence of adaptive thresholding on peaks detection in audio data. Digit. Signal Process. Multimed. Tools Appl. **79**, 19329–19348 (2020)
51. Y.W. Leung, Y.P. Wang, Multiobjective programming using uniform design and genetic algorithm. IEEE Trans. Syst. Man Cybern. C **30**(3), 293–304 (2000)
52. A. Papoulis, *Probability, Random Variables, and Stochastic Processes*, 3rd edn. (McGraw-Hill, New York, 1991), p. 48
53. X.L. Chen, J. Guan, Y. Huang, N.B. Liu, Y. He, Radon-linear canonical ambiguity function-based detection and estimation method for marine target with micromotion. IEEE Trans. Geosci. Remote Sens. **53**(4), 2225–2240 (2015)

Publisher's Note
Springer Nature remains neutral with regard to jurisdictional claims in published maps and institutional affiliations.